Int. J. Heat Mass Transfer. Vol. 15, pp. 969–987. Pergamon Press 1972. Printed in Great Britain

TWO-DIMENSIONAL STAGNATION POINT FLOWS OF BINARY MIXTURES*

A. F. MILLS and A. WORTMAN
University of California, Los Angeles, California, U.S.A.

(*Received* 15 *July* 1971 *and in revised form* 17 *September* 1971)

Abstract—Comprehensive numerical solutions have been obtained for axisymmetric and planar stagnation point flows of air with foreign gas injection. The injected species are H, H_2, He, C, CH_4, O, H_2O, Ne, Air, Ar, CO_2, Xe, CCl_4 and I_2, at wall cooling ratios of $T_s/T_e = 0{\cdot}1$, 0·5 and 0·9. Thermodynamic properties are calculated assuming an inert ideal gas mixture and constant species specific heats; for the transport properties the rigid sphere model is used in order to eliminate temperature level as a problem parameter. The effect of injectant thermodynamic and transport properties on the reduction, due to mass transfer, of wall shear stress, mass transfer conductance and heat transfer rate, are explained with the aid of results calculated for synthetic injectants with adjusted specific heats and collision cross-sections. The increased pressure gradient at planar points ($\beta = 1{\cdot}0$) is found to yield results little different to those for the axisymmetric situation ($\beta = 0{\cdot}5$), except for the shear stress reduction with light injectants at high wall temperatures. Thermal diffusion effects with moderate to severe wall cooling are found to be interesting, but of little practical importance. Engineering correlations for mass and heat transfer are presented. These are of the exponential form suggested by a Couette flow model, with the blowing parameter B weighted by the factors

$$a_{m,i} = 1{\cdot}65\left(\frac{M_{air}}{M_i}\right)^{\frac{1}{2}}; \qquad a_{h,i} = 1{\cdot}3\left(\frac{M_{air}}{M_i}\right)^{\frac{1}{4}}\left(\frac{C_{pi}}{\frac{5}{2}\mathscr{R}/M_i}\right)^{\frac{1}{4}}$$

for mass and heat transfer, respectively.

NOMENCLATURE

a, species weighting constant, equations (20) and (21);
B, blowing parameter $\equiv \dot{m}/g_h^*$ or $\dot{m}/g_{m,i}^*$;
$\mathscr{B}$, Spalding mass transfer driving force $\equiv \dot{m}/g_h$ or $\dot{m}/g_{m,i}$;
C, $\equiv \rho\mu/(\rho\mu)_e$;
C_p, specific heat;
$\mathscr{D}$, binary diffusion coefficient;
f, dimensionless stream function;
g, enthalpy ratio H/H_e, and conductance;
g_h, heat transfer conductance $\equiv q_s/(H_e - h_{es})$;
$g_{m,i}$, mass transfer conductance $\equiv j_{i,s}/(m_{i,s} - m_{i,e})$;
h, enthalpy;
H, total enthalpy;
j, species diffusive flux;
k, thermal conductivity;
Le, Lewis number $\equiv \rho C_p \mathscr{D}/k$;
M, molecular weight;
m, mass fraction;
$\dot{m}$, mass transfer rate;
N_{Av}, Avogadro's number;
p, pressure;
Pr, Prandtl number $= C_p\mu/k$;
q, conductive heat flux (including diffusional conduction if $\alpha_T \neq 0$);
$\mathscr{R}$, universal gas constant;
r, radius of an axisymmetric surface;
s, y, streamwise and normal coordinates, respectively;
Sc, Schmidt number $= \mu/\rho\mathscr{D}$;
St, Stanton number $= \rho_e u_e g$;
T, absolute temperature;
u, v, velocity components;
z_1, dimensionless mass fraction $\equiv m_1/m_{1,s}$;

* Computer time for the numerical calculations was supplied by the Campus Computing Network of the University of California, Los Angeles.

α_T, thermal diffusion factor;
β, pressure gradient parameter $\equiv d\ln u_e/d\ln\xi$;
ε, geometrical index;
η, transformed coordinate normal to the surface;
μ, dynamic viscosity;
ρ, density;
σ, collision diameter;
ξ, transformed coordinate along the surface;
τ, shear stress;
ψ, stream function.

Subscripts

e, free stream;
es, fluid of free stream composition at surface temperature;
h, heat transfer;
i, j, species i and j;
m, mass transfer;
o, reservoir;
s, surface (wall);
1, 2, injected and free stream species, respectively.

Superscripts

$'$, differentiation with respect to η;
$*, \cdot$ zero mass transfer;
t, total energy flux relative to mass average velocity.

INTRODUCTION

STAGNATION point flows with foreign gas injection have been the subject of numerous analytical studies. Of primary interest has been the reduction, due to mass transfer, of the wall shear stress, the mass transfer conductance and the heat transfer rate. The simplest situation is that of an inert binary mixture where species 1 is injected at the wall and the free stream contains species 2 only. Solutions to this problem are of fundamental importance to the theory of heat and mass transfer in laminar boundary layers; in addition such solutions find engineering application for the prediction of transpiration, evaporation and sublimation processes. The useful prior work is as follows. Baron [1] studied the influence of thermodynamic coupling on heat transfer for the injection of He and Freon 13 at an axisymmetric stagnation point. Data were obtained for an adiabatic wall and cooling ratios down to $T_s/T_e = 0{\cdot}4$. Sparrow *et al.* [2] considered the injection of H_2, He, A, CO_2 and Xe into air, using exact thermodynamic properties and transport properties based on the Lennard–Jones potential model. This study was also primarily concerned with the effects of thermal diffusion and diffusional conduction at adiabatic or nearly adiabatic conditions. Limited data were presented for cold wall conditions: for the axisymmetric stagnation point data were obtained for $T_s/T_e = 0{\cdot}25$, while for the planar stagnation point cold wall cases were not computed. Libby and Sepri [3] obtained data for the injection of He and Xe into N_2 at an axisymmetric stagnation point; although properties were modeled to eliminate temperature level as a parameter, only one value of the injectant reservoir temperature to free stream temperature (0·1) was considered. Related studies which are also pertinent are those of Anfimov [4] and Gomez *et al.* [5], who present data for injection of inert gases into equilibrium air for hypersonic flow at an axisymmetric stagnation point. Gollnick [6] experimentally studied diffusional conduction effects by measuring adiabatic wall temperatures and heat transfer rates on a porous hemisphere with He and Freon 13 injection.

The above mentioned work is difficult to use in fundamental studies of binary stagnation point flows owing to the diverse objectives, and the paucity of systematic data. The objective of the present work is to show clearly the effects of the problem parameters: comprehensive calculations have been performed, and the data presented in this paper are selected for their instructional value. The free stream is air while for axisymmetric flows the injected gases are

H, H_2, He, C, CH_4, O, H_2O, Ne, Air, Ar, CO_2, Xe, CCl_4 and I_2. This variety of species facilitates interpretation of the effects of injectant thermodynamic and transport properties on the wall shear stress, mass transfer conductance and heat transfer rate. Further illumination is provided by data obtained for synthetic injectants, fabricated from various molecules by replacing, in turn, their specific heat and collision cross-section by air values. Thermodynamic properties were calculated assuming an ideal gas mixture and constant species specific heats; for the transport properties the rigid sphere model was assumed. Thus temperature level was not a parameter of the problem. For each injectant, calculations were made for a range of values of T_s/T_e, in order to establish the effects of wall cooling. By performing detailed computations at low injection rates, the anomalous behavior of heat transfer with light gas injection established for turbulent flows [7] is clarified for laminar flows. Calculations, including the effects of thermal diffusion and diffusional conduction, were made for H, H_2, He, C and Xe, assuming that the thermal diffusion factor was independent of concentration and temperature. These results will not be emphasized owing to our simplifying assumptions, and the detailed study of such effects in [1, 2, 6]. For planar flows calculations were restricted to He, Air and Xe injectants; the resulting data is sufficient to allow a display of the essential differences between planar and axisymmetric stagnation point flows. Selected examples of velocity and enthalpy profiles will be presented to illustrate various interesting structural features of binary boundary layers. For example, velocity overshoots of up to a factor of two are found for H injection. Finally we will be concerned with the correlation of our data for engineering application.

ANALYSIS

The coordinate system is chosen such that s is measured along, and y perpendicular to the surface; the corresponding velocity components are u and v respectively. For steady, laminar, stagnation point flow of a binary gas mixture, the governing conservation equations are

mass:

$$\frac{\partial}{\partial s}(\rho u r^{\varepsilon}) + \frac{\partial}{\partial y}(\rho v r^{\varepsilon}) = 0 \tag{1}$$

momentum:

$$\rho u \frac{\partial u}{\partial s} + \rho v \frac{\partial u}{\partial y} = -\frac{\partial p}{\partial s} + \frac{\partial}{\partial y}\left(\mu \frac{\partial u}{\partial y}\right) \tag{2}$$

species:

$$\rho u \frac{\partial m_1}{\partial s} + \rho v \frac{\partial m_1}{\partial y} = -\frac{\partial}{\partial y}(j_1) \tag{3}$$

total enthalpy:

$$\rho u \frac{\partial H}{\partial s} + \rho v \frac{\partial H}{\partial y} = -\frac{\partial}{\partial y}(q^t). \tag{4}$$

The geometrical index ε assumes a value of 1 for an axisymmetric flow and 0 for a planar flow. The mass and energy flux vector are obtained from the Chapman–Enskog kinetic theory of gases [8] and are

$$j_1 = -\rho \mathscr{D}_{12}\left[\frac{\partial m_1}{\partial y} + m_1(1-m_1)\alpha_T \frac{\partial \ln T}{\partial y}\right] \tag{5}$$

$$q^t = -k\frac{\partial T}{\partial y} + j_1\left[h_1 - h_2 + \alpha_T \frac{M}{M_1 M_2}\mathscr{R}T\right]. \tag{6}$$

The boundary conditions imposed on the set of equations are

$$y = 0: \quad u = 0; \quad \rho v = \dot{m};$$

$$\dot{m} = m_{1,s}\dot{m} + j_1|_s; \quad T = T_s \tag{7}$$

$$y \to \infty: \quad u \to u_e; \quad m_1 \to 0; \quad H \to H_e. \tag{8}$$

Following Lees [9] the transformation $s, y \to \xi, \eta$ is made where the Levy and Mangler transformations have been combined in defining

$$\eta = \frac{\rho_e u_e}{(2\xi)^{\frac{1}{2}}}\int_0^y r^{\varepsilon}\frac{\rho}{\rho_e}\,dy \tag{9}$$

$$\xi = \int_0^s \rho_e \mu_e u_e r^{2\varepsilon}\,ds. \tag{10}$$

A stream function ψ is introduced such that

$$\rho u r^{\varepsilon} = \frac{\partial \psi}{\partial y} \qquad \rho v r^{\varepsilon} = -\frac{\partial \psi}{\partial s} \tag{11}$$

and choosing $\psi(\xi, \eta) = (2\xi)^{\frac{1}{2}} f(\eta)$ leads to

$$\frac{u}{u_e} = \frac{\partial f}{\partial \eta} = f'. \tag{12}$$

Under this transformation the governing equations for stagnation point flows are, in non-dimensional form,

$$(Cf'')' + ff'' = \beta\left(f'^2 - \frac{\rho_e}{\rho}\right) \tag{13}$$

$$\left(\frac{C}{Sc} z_1'\right) + f z_1' = -\left[\frac{C}{Sc} z_1 (1 - m_1)\alpha_T \frac{T'}{T}\right]' \tag{14}$$

$$\left(\frac{C}{Pr} g'\right)' + fg'$$
$$= \left[\frac{C}{Sc}(g_1 - g_2) m_{1,s} \left\{ z_1' \left(\frac{1}{Le} - 1\right) - z_1 (1 - m_1)\alpha_T \frac{T'}{T} \right\}\right]' - \left[\frac{C}{Sc}\alpha_T \frac{\mathscr{R}TM}{M_1 M_2} m_{1,s} \times \left\{ z_1' + z_1 (1 - m_1)\alpha_T \frac{T'}{T} \right\}\right]' \tag{15}$$

which are to be solved subject to the boundary conditions

$$\eta = 0: \quad f = f_s, \quad f' = 0, \quad m_{1,s} = \left.\frac{f}{f + \frac{C}{Sc}\left[z_1' + z_1 (1 - m_1)\alpha_T \frac{T'}{T}\right]}\right|_{\eta = 0}, \quad g = g_s^* \tag{16}$$

$$\eta \to \infty: \quad f' \to 1, \quad z_1 \to 0, \quad g \to 1. \tag{17}$$

The pressure gradient parameter β assumes a value of $\frac{1}{2}$ for axisymmetric stagnation points and 1 for planar ones.

Thermodynamic and transport properties

The mixture thermodynamic properties were computed assuming an ideal gas mixture and constant species specific heats. The species viscosity, thermal conductivity and binary diffusion coefficients were computed assuming a rigid sphere molecular interaction model, viz.

$$\mu_i = \frac{5}{16}\left(\frac{\mathscr{R}TM_i}{\pi}\right)^{\frac{1}{2}} \frac{1}{N_{Av}\sigma_i^2}$$

$$k_i = \mu_i \left(C_{pi} + \frac{5}{2}\frac{\mathscr{R}}{M_i}\right)$$

$$\rho \mathscr{D}_{ij} = \frac{3}{8}\left(\frac{\mathscr{R}T}{\pi}\right)^{\frac{1}{2}} \left(\frac{M_i + M_j}{2M_i M_j} \frac{M}{N_{Av}(\sigma_i + \sigma_j/2)^2}\right) \tag{18}$$

and the mixture rules are, following [8]

$$\mu = \sum_{j=1}^{2} \frac{x_j \mu_j}{\sum_{k=1}^{2} x_j G_{jk}}; \qquad k = \sum_{j=1}^{2} \frac{x_j k_j}{\sum_{k=1}^{2} x_j G_{jk}} \tag{19}$$

where

$$G_{jk} = 1{\cdot}154\left(\frac{1 + \sigma_k/\sigma_j}{2}\right)^2 \left(\frac{2}{M_j/M_k + 1}\right)^2 \quad j \neq k$$
$$= 1{\cdot}0. \qquad j = k$$

The molecular weights, collision cross-sections and specific heats were obtained from [10–12] and are listed in Table 1. In estimating properties in this manner our objective was to eliminate temperature level as a problem parameter. Consequently, in those calculations where thermal diffusion and diffusional conduction were included, the thermal diffusion factor was also

Table 1. Thermodynamic and transport properties of the injected gases

Species	M	$\frac{M}{M_{air}}$	$\frac{\sigma}{\sigma_{air}}$	$\frac{C_p}{C_{p\,air}}$	$\frac{\mu}{\mu_{air}}$	$\frac{k}{k_{air}}$	Sc_e
H	1·008	0·03480	0·7410	20·48	0·340	7·693	0·164
H_2	2·016	0·06959	0·8059	14·21	0·406	5·786	0·245
He	4·003	0·1382	0·7122	5·156	0·733	4·177	0·301
C	12·01	0·4146	0·7741	1·723	1·075	2·045	0·502
CH_4	16·04	0·5537	1·050	2·211	0·675	1·421	0·739
O	16·00	0·5523	0·8018	1·359	1·156	1·708	0·570
H_2O	18·02	0·6219	0·7808	1·851	1·294	2·311	0·578
Ne	20·18	0·6966	0·7902	1·023	1·337	1·511	0·605
Air	28·97	1·000	1·000	1·000	1·000	1·000	0·833
Ar	39·94	1·379	0·9458	0·5168	1·313	0·750	0·849
CO_2	44·01	1·519	1·093	0·8396	1·032	0·816	1·002
Xe	131·3	4·532	1·121	0·1570	1·694	0·294	1·200
CCl_4	153·8	5·309	1·651	0·5378	0·845	0·377	1·900
I_2	253·8	8·761	1·432	0·1443	1·443	0·197	1·651

taken to be independent of temperature. In addition, since data for α_T is basically unreliable, it was also taken to be independent of concentration. The constant values of α_T employed were chosen based on data calculated from the Kihara formula with the Lennard–Jones potential [8].

Solution procedure

The method of solution employed in the

Table 2. Comparison of data calculated in the present study with that of Libby and Sepri [3], $\beta = 0{\cdot}5$. *Properties as in* [3]; *the numerical data was kindly supplied by Professor P. A. Libby in a personal communication*

		He → N_2					
		Present study			Libby and Sepri [3]		
$-f_s$	T_s/T_e	$C_s f_s''$	$\frac{C_s}{Pr_s} g_s'$	$m_{1,s}$	$C_s f_s''$	$\frac{C_s}{Pr_s} g_s'$	$m_{1,s}$
0·1	0·6309	0·8029	0·2265	0·1030	0·7985	0·2198	0·1017
0·3	0·3476	0·6012	0·3186	0·4495	0·5964	0·3076	0·4504
0·5	0·2220	0·4427	0·2630	0·8145	0·4404	0·2525	0·8155
0·7	0·1568	0·3209	0·1717	0·9670	0·3201	0·1647	0·9669
0·9	0·1237	0·2332	0·09197	0·9965	0·2329	0·08847	0·9965
		Xe → N_2					
0·1	0·9815	0·8841	0·01121	0·1755	0·8819	0·01112	0·1757
0·3	0·9411	0·8022	0·03219	0·4116	0·7971	0·03183	0·4117
0·5	0·8959	0·7267	0·05123	0·5614	0·7199	0·05020	0·5617
0·7	0·8462	0·6572	0·06795	0·6635	0·6498	0·06589	0·6643
0·9	0·7922	0·5931	0·08186	0·7368	0·5856	0·07857	0·7378
1·1	0·7341	0·5339	0·09271	0·7913	0·5264	0·08798	0·7936
1·3	0·6733	0·4794	0·09905	0·8336	0·4725	0·09401	0·8354
1·5	0·6104	0·4289	0·1017	0·8667	0·4228	0·09657	0·8686
1·7	0·5471	0·3824	0·1007	0·8932	0·3771	0·09587	0·8948
1·9	0·4840	0·3395	0·09657	0·9145	0·3353	0·09202	0·9157

present study was developed in [13], where it was applied to the calculation of a wide range of boundary layer problems. Formal integration of equations (13)–(15), subject to the boundary conditions, yields a relation which may be written in functional form as $X = FX$, where F is an operator on X, and is itself a function of X since it depends on the basic functions in the conservation equations; X is the solution vector whose components are the principal dependent variables of the conservation equations. The solution procedure is an iterative one. Special care is taken to restrict the range of the operator which ensures establishment of a converging sequence by forcing successive solutions into a region where the Banach fixed point theorem applies. Weighted averaging of successive solutions satisfactorily restricted the operator range for all the cases considered in this paper. The analytical nature of the solution made programming a simple matter of organizing the variables and evaluating the required integrals. All the integrals are well behaved functions so that Simpson's rule was sufficiently accurate for the quadratures. The number of integration steps across the boundary layer was 151 in all cases. Computer time (IBM 360/65 system) was typically 4 s per solution for four place accuracy. Additional discussion of the method may be found in [13, 14], where the accuracy and reliability of the method is demonstrated for several different classes of problem. Table 2 presents a comparison with calculations of Libby and Sepri [3], and confirms that our method is reliable for foreign gas injection.

RESULTS AND DISCUSSION

The situations computed were as follows. For the axisymmetric stagnation point ($\beta = 0{\cdot}5$) the injectants were: H, H_2, He, C, CH_4, O, H_2O, Ne, Air, Ar, CO_2, Xe, CCl_4 and I_2. For the planar stagnation point ($\beta = 1{\cdot}0$) the injectants were He, Air and Xe. The synthetic injectants were constructed from He, C, CH_4 and Xe by setting, in turn, (i) $\sigma = \sigma_{air}$, (ii) $C_p = C_{p\,air}$, and (iii) $\sigma = \sigma_{air}$, $C_p = C_{p\,air}$. The effects of thermal diffusion and diffusional conduction were studied at $\beta = 0{\cdot}5$ for the injectants H, H_2, He, C and Xe. For all cases three values

Table 3. Data for selected cases; complete tabulations are to be found in [14]

Injectant	β	T_s/T_e	$-f_s$	$C_s f''_s$	$\frac{C_s}{Pr_s} g'_s$	$-\frac{C_s}{Sc_s} z'_s$	C_s	Pr_s	Sc_s
H_2	0·5	0·1	0	0·7555	0·6509	1·3721	3·1623	0·7402	0·2451
H_2	0·5	0·1	0·5	0·1359	0·0533	0·0068	0·0909	0·7335	1·4198
H	0·5	0·1	0·05	0·5959	0·7044	1·0960	1·2838	0·3382	0·3248
H	0·5	0·1	0·5	0·1125	0·0167	0·0001	0·0374	0·6693	1·5991
He	0·5	0·1	0·5	0·2724	0·2315	0·0899	0·3778	0·6258	1·4207
He	0·5	0·9	0	0·9101	0·0654	1·1271	1·0541	0·7402	0·3010
CH_4	0·5	0·9	0·5	0·5774	0·0205	0·0637	0·1204	0·6369	1·4663
H_2O	0·5	0·1	0·5	0·4482	0·3600	0·3934	2·5758	0·7218	0·8464
H_2O	0·5	0·9	0·5	0·6711	0·0339	0·3241	0·8535	0·7243	0·8778
CO_2	0·5	0·1	0·5	0·4679	0·3822	0·3876	3·7135	0·7542	0·7641
CO_2	0·5	0·9	0·5	0·6207	0·0366	0·3359	1·2585	0·7563	0·7571
Xe	0·5	0·1	1·5	0·3074	0·2421	0·2355	14·3570	0·5880	0·5761
Xe	0·5	0·9	1·0	0·5667	0·0349	0·2887	3·6602	0·5839	0·6526
CCl_4	0·5	0·9	1·0	0·4208	0·0249	0·2153	2·7572	0·7178	0·5558
He	1·0	0·1	0	0·8820	0·6700	1·2451	3·1623	0·7402	0·3010
He	1·0	0·1	1·0	0·2295	0·0388	0·0012	0·3206	0·6690	1·5947
He	1·0	0·9	0	1·1999	0·0688	1·1739	1·0541	0·7402	0·3010
He	1·0	0·9	0·8	0·7746	0·0089	0·0091	0·1080	0·6661	1·5831
Xe	1·0	0·9	2·0	0·6219	0·0194	0·1834	5·6993	0·6008	0·5307

of the ratio T_s/T_e were considered: 0·1, 0·5 and 0·9. In all, over 1200 solutions were obtained. In [13] can be found complete tabulations of the quantities

(i) the wall shear stress function $C_s f''_s$;
(ii) the wall conductive heat flux function $C_s g'_s/Pr_s$;
(iii) the mass transfer conductance function $C_s z'_s/Sc_s$;
(iv) the wall value of the injectant mass fraction, $m_{1,s}$;
(v) the wall value of $\rho\mu/(\rho\mu)_e = C_s$;
(vi) the wall value of the Prandtl number, Pr_s;
(vii) the wall value of the Schmidt number, Sc_s.

Table 3 contains a selection of data, including some of the cases which proved more difficult to compute; these data might be useful to other workers for evaluation of accuracy and reliability.

The essential characteristics of the data may be understood on the basis of the assessment of binary boundary layer flows made by Gomez, Mills and Curry [4]. The effect of like species injection (e.g. air into air) in reducing momentum, mass and heat transfer is revealed by constant property solutions. Foreign gas injection yields reductions different to those obtained for like species injection due to the effect of composition on mixture transport and thermodynamic properties. A complex coupling of the conservation equations results from the property variations across the boundary layer, and it is only possible to explain the major trends exhibited by the data. Property variations influence the momentum conservation equation most strongly through the $(\rho\mu)$ product, or equivalently, through $C = (\rho\mu)/(\rho\mu)_e$. The effect is similar to the response of a compressible boundary layer with no injection, to changes in wall

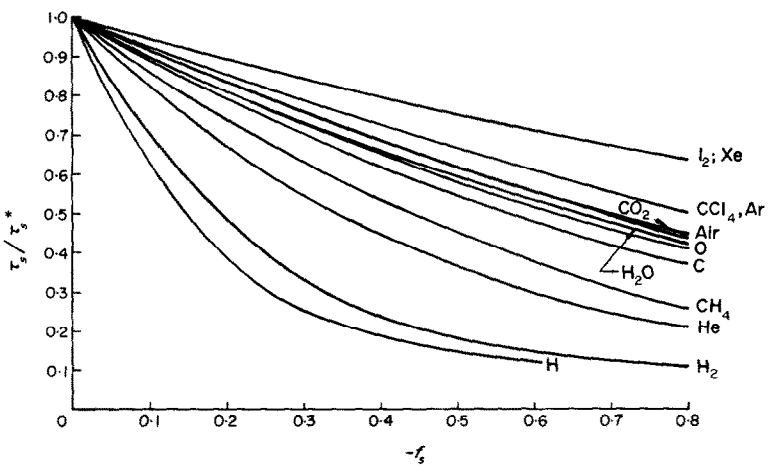

FIG. 1. Effect of mass transfer on wall shear stress. $\beta = 0{\cdot}5$; $T_s/T_e = 0{\cdot}1$.

Effect of injected species

Figures 1–3 show the shear stress $\tau_s = \mu\partial u/\partial y|_s$, mass transfer conductance $g_m = j_{1,s}/(m_{1,s} - m_{1,e})$, and conductive heat flux $q_s = k\partial T/\partial y|_s$, each normalized by their respective zero mass addition values, at an axisymmetric stagnation point under "cold wall' conditions ($g_s = 0{\cdot}1$). temperature, for which it is well known that the wall shear stress is proportional to C_s raised to an exponent of about 0·1. Density is directly proportional to molecular weight; viscosity tends to increase weakly and somewhat irregularly with molecular weight. Thus C_s tends to increase with molecular weight of the

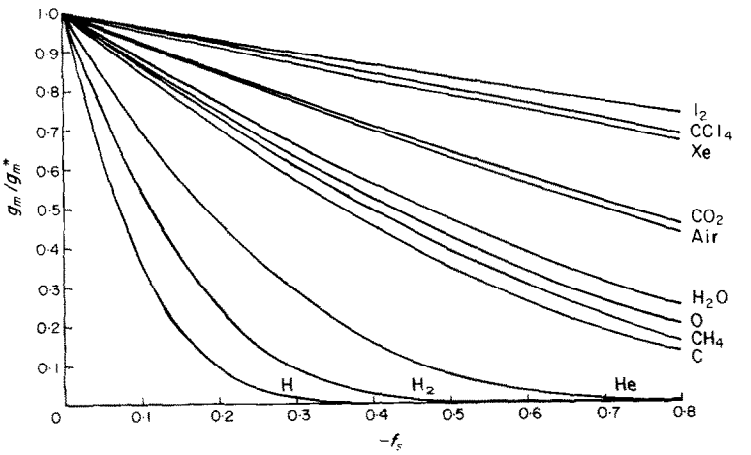

FIG. 2. Effect of mass transfer on mass transfer conductance.
$\beta = 0{\cdot}5$; $T_s/T_e = 0{\cdot}1$.

injected species, though account must be taken of the fact that mixture thermodynamic properties vary with the mass fractions of the components, whereas mixture transport properties vary approximately with the mole fractions. For a given mass injection rate ($-f_s$), the wall mole fraction $x_{1,s}$ is typically much larger for a light injectant than for a heavy one. Thus, whereas the viscosity of a light injectant does have some effect on C_s, for a heavy injectant C_s is essentially determined by the injectant density. Figure 4a confirms this point; when the values of σ for C and Xe are replaced by the value for air, we see that τ_s/τ_s^* is significantly affected for the light injectant only. Furthermore, when σ_C is replaced by σ_{air}, the value of C_s at, for example, $-f_s = 0{\cdot}5$ changes from 1·700 to 1·231; the accompanying reduction in shear confirms the suggested effect of C_s. A primary ($\rho\mu$) effect has therefore been identified which

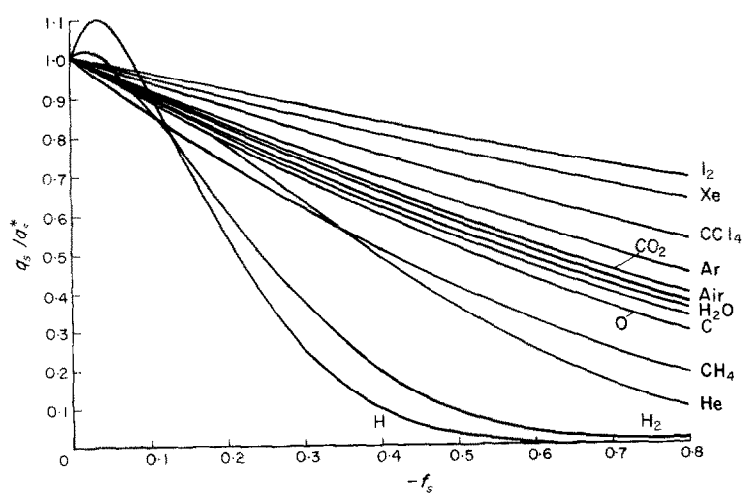

FIG. 3. Effect of mass transfer on heat transfer rate. $\beta = 0{\cdot}5$;
$T_s/T_e = 0{\cdot}1$.

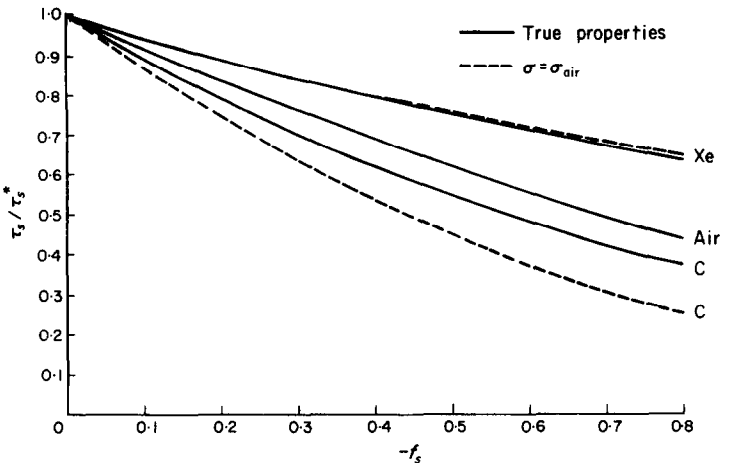

FIG. 4a. Effect of injectant collision cross-section on wall shear stress. $\beta = 0{\cdot}5$; $T_s/T_e = 0{\cdot}1$.

results in light injectants being most effective in reducing shear stress. Turning to heat transfer, the $(\rho\mu)$ effect can be isolated, as again, for compressible boundary layers, it is known that at constant Prandtl number the heat transfer is approximately proportional to $C_s^{0{\cdot}1}$. It also follows that, for a constant Schmidt number, the reduction of the mass transfer conductance behaves in a similar manner.

In ascertaining the effects of non-constant Prandtl and Schmidt numbers, it is easiest to first consider the mass transfer conductance. The Schmidt number is a measure of the relative rates of transport of momentum and species. Since $Sc = \mu/\rho\mathscr{D}_{12}$, and $\mathscr{D}_{12}$ is composition independent, the value of Sc_s is decreased for heavy injectants via the density; for light injectants this effect is weakly and irregularly counteracted via the viscosity. Thus the primary $(\rho\mu)$ effect is strongly augmented by a Schmidt number effect which, especially for heavy injectants, is essentially a density effect. In fact it will be seen that the mass transfer conductance can be well correlated in terms of the molecular

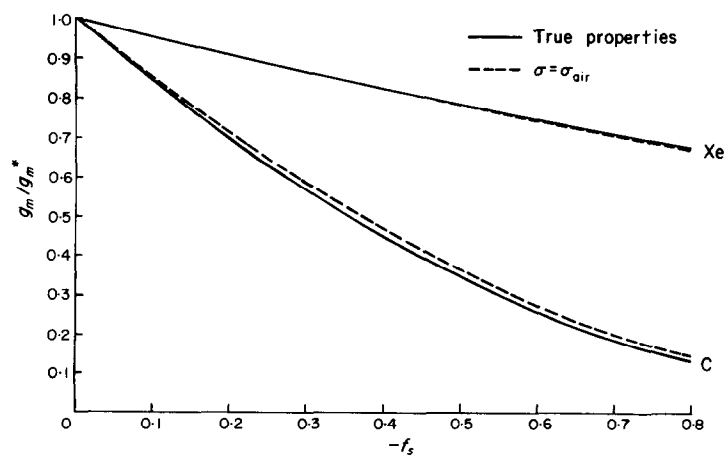

FIG. 4b. Effect of injectant collision cross-section on mass transfer conductance. $\beta = 0{\cdot}5$; $T_s/T_e = 0{\cdot}1$.

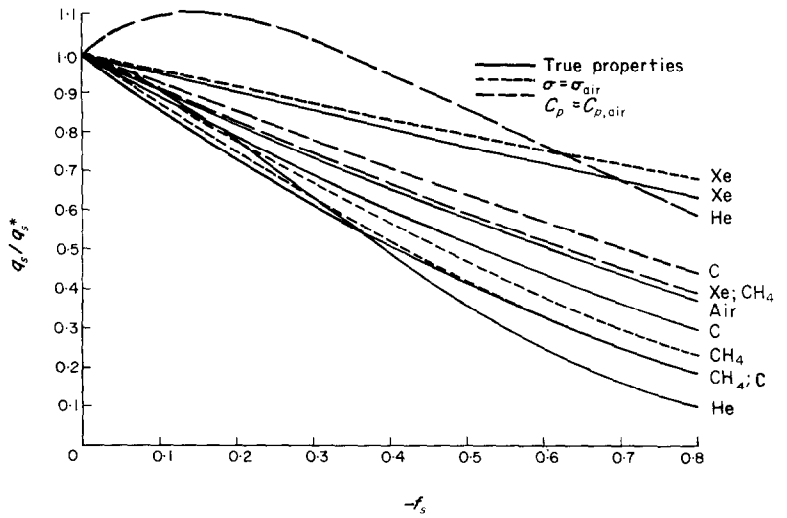

FIG. 4c. Effects of injectant collision cross-section and specific heat on heat transfer rate. $\beta = 0{\cdot}5$; $T_s/T_e = 0{\cdot}1$.

weight of the injectant. Figure 4b shows how, even for the light injectant C, the effect of setting $\sigma_C = \sigma_{air}$ is negligible; Sc is independent of σ so that the change in σ is felt only indirectly through the $(\rho\mu)$ product. The heat transfer behavior is more complex. The Prandtl number is a measure of the relative rates of transport of momentum and energy. We have $Pr = C_p\mu/k$, both k and C_p increase with decreasing molecular weight, but C_p more strongly so; in addition, C_p increases with the complexity of the molecule. The weak and irregular increase of μ with molecular weight has an insignificant effect on Pr. Again the transport property k plays a more important role for light injectants owing to the associated large values of $x_{1,s}$. Thus the effect of Prandtl number is to augment the primary $(\rho\mu)$ effect, but not as strongly as was the case for the Schmidt number. Figure 4c illustrates well the counteracting effects of k and C_p for He; when $C_{p\,He}$ is set equal to $C_{p\,air}$ we see a dramatic increase in heat transfer accompanying the lower Prandtl number. The values of q_s/q_s^* greater than unity, shown in Fig. 3, are similarly explained: at low injection rates the wall mole fractions of the light injectants H and H_2 are much greater than their mass fractions, thus although k_s is markedly changed, the value for C_{ps} remains almost equal to the value for air. At higher injection rates $m_{1,s}$ as well as $x_{1,s}$ approach unity and the C_p effect dominates. Also illustrated in Fig. 4c is the effect of the $(\rho\mu)$ product: when σ_C is set equal to σ_{air} there is a decrease in the heat transfer, while when σ_{CH_4} is set equal to σ_{air} there is an increase. Although C and CH_4 both have molecular weights less than air, $\sigma_C < \sigma_{air}$ while $\sigma_{CH_4} > \sigma_{air}$ (see Table 1). The calculated values for C_s are found to be in line with these arguments.

Based on the foregoing assessment of binary boundary layer flows, and the data presented in Table 1, the following additional comments on the important features of Figs. 1–3 are offered:

(1) Referring to Fig. 1, I_2 is as effective as Xe in reducing the surface shear stress. The lower viscosity of I_2 modifies the primary density effect. A similar statement can be made in comparing CCl_4 with Ar as well as for CO_2 and air. Although their molecular weights are identical, CH_4 is more effective than O due to the lower viscosity of CH_4.

(2) Referring to Fig. 2, the effectiveness of the injectants in reducing the mass transfer conductance exhibits a quite regular be-

havior with molecular weight.

(3) Comparing Figs. 1–3 it is seen that the effect of injectant molecular weight is most pronounced in Fig. 2; this feature confirms the direct augmentation of the primary density dependence by the additional density dependence of the mass exchange coefficient $\rho\mathscr{D}_{12}$.

(4) Referring to Fig. 3 the marked effect of the lightest injectants, H, H_2 and He in increasing the mixture thermal conductivity adjacent to the wall is clearly shown. The blowing and primary ($\rho\mu$) effects are overwhelmed at small values of $-f_s$.

(5) CCl_4 is more effective than Xe in reducing heat transfer, as its much higher specific heat reverses the primary density effect. A similar statement applies in comparing CO_2 and Ar, as well as for CH_4 in relation to O and CO.

(6) The relative effectiveness of CH_4 and He in reducing heat transfer is particularly interesting. At low values of $-f_s$, He is less effective due to the higher thermal conductivity of the He–air mixture adjacent to the wall. At larger values of $-f_s$ the higher specific heat and lower density of helium dominates and He is more effective than CH_4.

Effect of temperature ratio

Figure 5a shows the effect of wall temperature ratio T_s/T_e on the reduction, due to mass transfer, of the wall shear stress. The ratio τ_s/τ_s^* is seen to increase with increasing wall temperature; this behavior is opposite to that found for zero pressure gradient flows ($\beta = 0$, flat plate or conical), as shown, for example, in [13]. In the absence of a pressure gradient the temperature ratio enters the problem only through the effect on the variation of $C = \rho\mu/(\rho\mu)_e$ across the flow. Increased wall temperatures lead to decreased values of C_s and hence decreased values of τ_s. Normalization with τ_s^* does not completely remove the effect of T_s/T_e owing to the distortion of the C-profile by mass transfer; the flattening of the profile near the wall extends the influence of the wall value of C further into the boundary layer. In contrast for $\beta = 0{\cdot}5$ both τ_s and τ_s/τ_s^* increase with increasing wall temperature, due to the effect of wall temperature on the density ratio ρ_e/ρ, which only enters the problem for $\beta \neq 0$. An examination of equation (13) shows that a decrease in ρ_e/ρ, as would be caused by an increase in T_s/T_e, increases the shear stress. At $\beta = 0{\cdot}5$ the effect of T_s/T_e on ρ_e/ρ outweighs its effect on C to yield the observed trends.

Figures 5b and 5c show the effect of wall

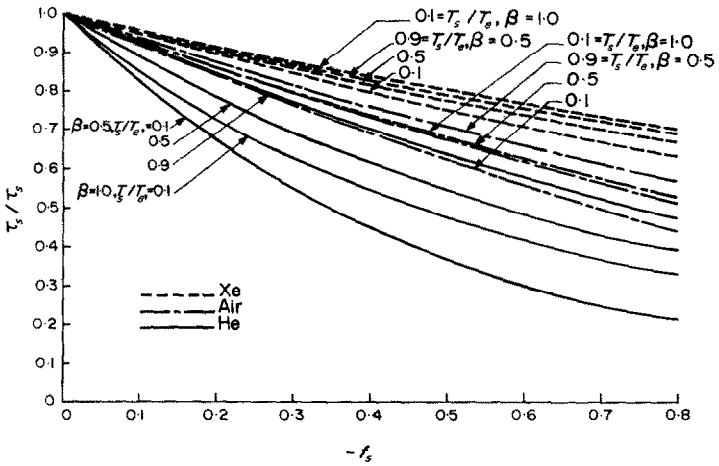

FIG. 5a. Effects of wall cooling and pressure gradient on wall shear stress.

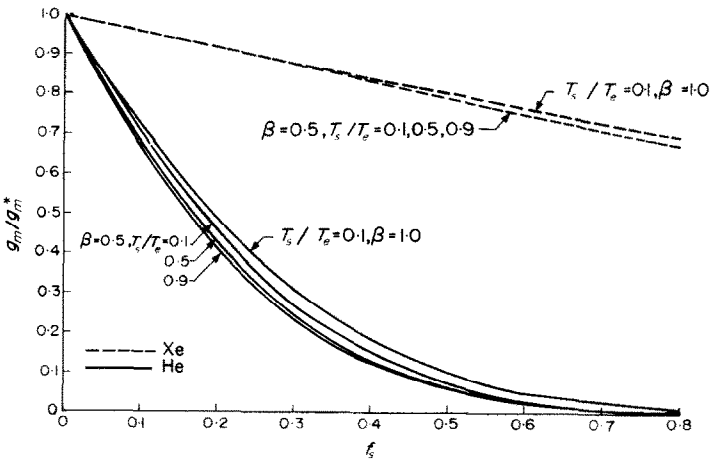

FIG. 5b. Effects of wall cooling and pressure gradient on mass transfer conductance.

temperature on the reduction due to mass transfer of, respectively, the mass transfer conductance and the heat transfer. Both the ratios g_m/g_m^* and q_s/q_s^* decrease with increasing wall temperature. The decreases are not as marked as those found for $\beta = 0$ flows, e.g. as shown in [13]. It appears that the effect of temperature ratio on C dominates the behavior of the species and energy equations, with only a secondary effect of the density ratio being felt.

Effect of pressure gradient

Also shown in Figs. 5a, b and c are the effects of pressure gradient, i.e. the differences between axisymmetric ($\beta = 0{\cdot}5$) and planar ($\beta = 1{\cdot}0$) stagnation point flows. Data are shown for one value of the temperature ratio, $T_s/T_e = 0{\cdot}1$; the observed trends are independent of temperature ratio, except for the shear stress with light injectants. The ratios of τ_s/τ_s^*, g_m/g_m^* and q_s/q_s^* all increase with pressure gradient, the effect being most marked for τ_s/τ_s^*. Comments similar to those made above for the effect of wall temperature ratio apply here as well. The values of τ_s^*, g_m^* and q_s^* all increase with increasing β, as is most easily seen for the shear stress upon

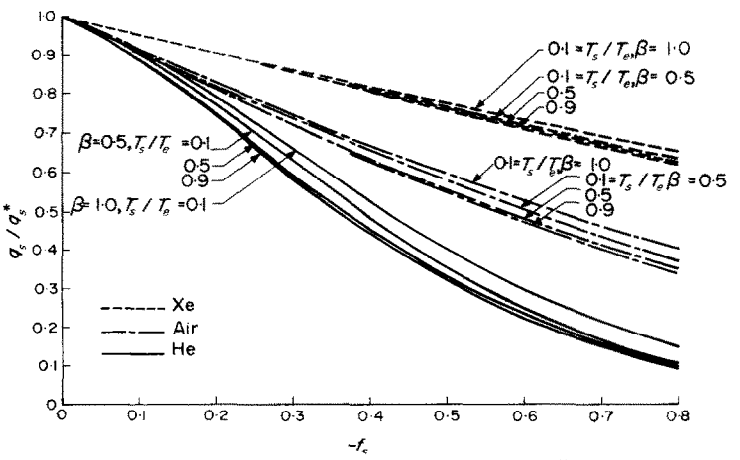

FIG. 5c. Effects of wall cooling and pressure gradient on heat transfer rate.

examination of equation (13). A more marked effect for light gas injectants at high wall temperatures is also indicated; in physical terms, the pressure gradient is more easily able to accelerate a low density boundary layer.

Effects of diffusional conduction and thermal diffusion

The effects of diffusional conduction on the adiabatic wall temperature, and on heat transfer at moderate temperature ratios ($T_s/T_e = 0{\cdot}25 - 1{\cdot}1$), have been analysed by Baron [1] and Sparrow *et al.* [2]. Experimental confirmation has been provided by Gollnick [6]. The data that we have selected to present here are for the more severe wall cooling characteristic of ablation, where typical species of interest are H and C. The values of the thermal diffusion factor α_T used were $-0{\cdot}4$ for atomic hydrogen and $-0{\cdot}2$ for monatomic carbon vapor. Figure 6 shows the dimensionless conductive heat flux for $\alpha_T = 0$, $q_s (= C_s g'_s/Pr_s)$, together with data points for the total conductive flux including diffusional conduction. The results for $T_s/T_e = 0{\cdot}5$ exhibit the augmentation of ordinary

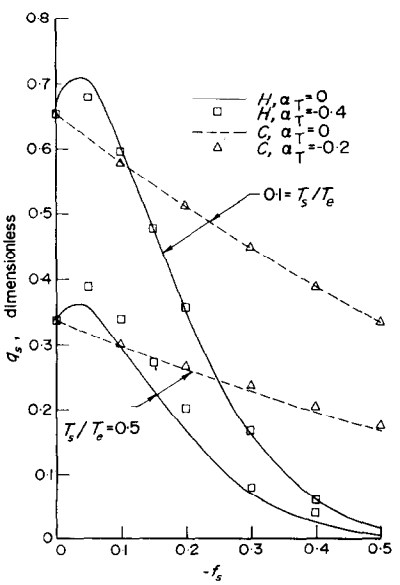

FIG. 6. Effects of diffusional conduction on heat transfer rate. $\beta = 0{\cdot}5$.

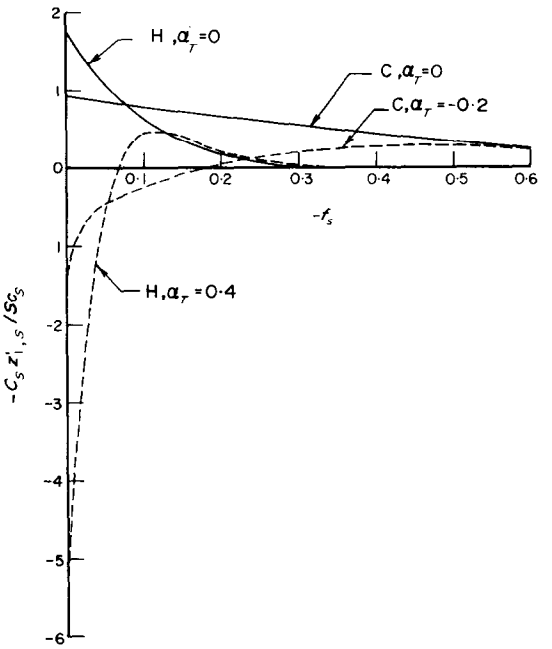

FIG. 7. Effects of thermal diffusion on the wall mass fraction gradient. $\beta = 0{\cdot}5$; $T_s/T_e = 0{\cdot}1$.

conduction by diffusional conduction expected for injectants possessing negative thermal diffusion factors. For $T_s/T_e = 0{\cdot}1$ the effect of $\alpha_T \neq 0$ for C is quite negligible; however, for H the effect of $\alpha_T \neq 0$ is to produce a decrease in the total conductive flux. Inspection of the numerical data showed that this anomaly is associated with decreased ordinary conduction due to thermal diffusion lowering $m_{1,s}$, and hence k_s.

In Fig. 7 there is shown the effects of thermal diffusion on the dimensionless wall mass fraction gradient $-C_s z'_s/Sc_s$ (which is the dimensionless mass transfer conductance for $\alpha_T = 0$). At low injection rates inclusion of thermal diffusion results in positive values of z'_s and associated maxima in the injectant concentration profiles. The thermal diffusion flux is directed away from the wall and is large enough to distort the concentration profile to the extent of yielding an anomalous positive value of $z'_{1,s}$, ordinary diffusion is thus directed towards the wall. This phenomena can occur during

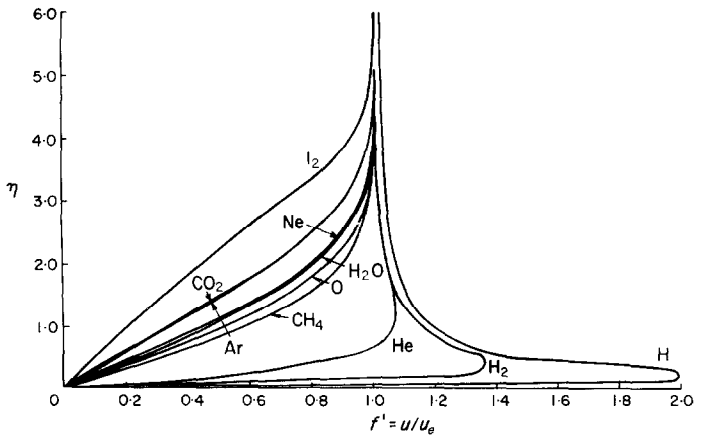

FIG. 8. Velocity profiles at an axisymmetric stagnation point. $T_s/T_e = 0{\cdot}5$; $-f_s = 0{\cdot}5$.

ablation under particular thermochemical conditions; it is of interest but the resulting effects are not large enough to be of practical consequence.

Velocity and enthalpy profiles

Figure 8 shows typical velocity profiles for the various injectants at $T_s/T_e = 0{\cdot}5$, for an injection rate of $-f_s = 0{\cdot}5$. Of particular interest are the marked velocity overshoots for the light injectants, even though there is substantial wall cooling. An overshoot of 100 per cent is observed for atomic hydrogen, while even helium exhibits a 7 per cent overshoot. Hoshizaki and Smith [15] computed data for helium injection by numerically integrating in the velocity plane (Crocco transformation); in so doing it was necessary to suppress velocity overshoots. The present results show that such a constraint is inadmissable for helium injection. Figure 9 shows enthalpy profiles at various injection rates for H_2 injection at $T_s/T_e = 0{\cdot}5$. The character of the profiles is as expected; the dramatic increase of wall enthalpy with injection is clearly seen.

Correlation of mass and heat transfer data

Of primary engineering interest at stagnation points is the prediction of mass and heat transfer rates. Following Gomez *et al.* [5] we use the exponential correlation functions suggested by Couette flow modeling of the boundary layer,

$$\frac{g_{m,i}}{g^*_{m,i}} = \frac{a_{m,i}B_{m,i}}{\exp(a_{m,i}B_{m,i}) - 1}; \quad B_{m,i} = \frac{\dot{m}}{g^*_{m,i}} \tag{20}$$

$$\frac{g_h}{g^*_h} = \frac{a_{h,i}B_h}{\exp(a_{h,i}B_h) - 1}; \quad B_h = \frac{\dot{m}}{g^*_h} \tag{21}$$

where

$$g_{m,i} = \frac{j_{i,s}}{m_{i,s} - m_{i,e}} = \rho_e u_e St_m \tag{22}$$

$$g_h = \frac{q_s}{H_e - h_{es}} = \rho_e u_e St_h. \tag{23}$$

Equations (20) and (21) are equivalent to the Spalding form [16, 17]

$$\frac{g}{g^*} = \frac{\ln(1 + a\mathscr{B})}{a\mathscr{B}}, \quad \mathscr{B} = \frac{\dot{m}}{g}; \tag{24}$$

modified by the inclusion of species weighting factors a. Appropriate values of $a_{m,i}$ and $a_{h,i}$ were empirically determined for each combination of injectant species, β and T_s/T_e by a least squares technique. Some discretion was used in the selection of data points to ensure a best fit in the range $1{\cdot}0 > g/g^* > 0{\cdot}25$. The exponential functions were found to fit the data well, with the exception of heat transfer for the light

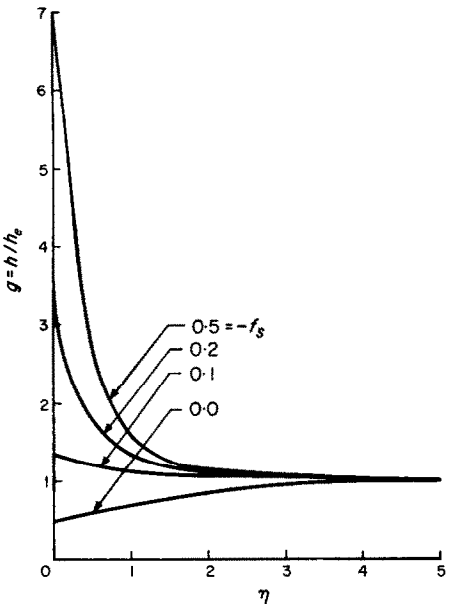

FIG. 9. Enthalpy profiles for H_2 injection at an axisymmetric stagnation point. $T_s/T_e = 0{\cdot}5$.

injectants H, H_2 and He. Examination of Fig. 3 suggests that the abnormally high values of q_s/q_s^* at low injection rates cannot be correlated in a simple manner. Direct use of graphical or numerical results is indicated for such situations, if high accuracy is desired. Table 4 lists the values of species weighting constants. Figures 10 and 11 show, respectively, plots of $a_{m,i}$ and $a_{h,i}$; for clarity data points showing the effect of wall cooling are omitted when the effect is small.

Our discussion of the effect of injectant species on the mass transfer conductance suggests that it should be possible to correlate $a_{m,i}$ in terms of molecular weight of the injectant. In Fig. 10 it is seen that the data are indeed well correlated by the expression

$$a_{m,i} = 1{\cdot}65\left(\frac{M_{\text{air}}}{M_i}\right)^{\frac{1}{6}}. \tag{25}$$

The correlation of the heat transfer weighting constants $a_{h,i}$ is not as simple. For monatomic molecules the ordinate in Fig. 11 is just $a_{h,i}$, and for monatomic injectants the data are satisfactorily correlated by

$$a_{h,i} = 1{\cdot}3\left(\frac{M_{\text{air}}}{M_i}\right)^{\frac{1}{3}}, \tag{26}$$

where the one-third power is well established in the literature [18]. To account for the effect of the higher values of C_p which characterize

Table 4. Species weighting constants $a_{m,i}$ *and* $a_{h,i}$, *to be used in equations* (20) *and* (21), *respectively*

Injectant	β	$T_s/T_e = 0{\cdot}1$		$T_s/T_e = 0{\cdot}5$		$T_s/T_e = 0{\cdot}9$	
		$a_{m,i}$	$a_{h,i}$	$a_{m,i}$	$a_{h,i}$	$a_{m,i}$	$a_{h,i}$
H	0·5	31·5	4·57	32·8	4·29	34·4	2·45
H_2	0·5	15·8	3·88	16·7	3·89	16·7	3·90
He	0·5	8·75	2·42	9·07	2·41	9·03	2·30
C	0·5	3·31	1·79	3·34	1·77	3·32	1·73
CH_4	0·5	2·38	2·32	2·40	2·33	2·38	2·31
O	0·5	2·62	1·69	2·57	1·66	2·55	1·61
H_2O	0·5	2·33	1·62	2·36	1·62	2·34	1·60
Air	0·5	—	1·56	—	1·54	—	1·52
Ne	0·5	2·16	1·51	2·15	1·47	2·12	1·44
Ar	0·5	1·22	1·32	1·18	1·27	1·15	1·25
CO_2	0·5	1·07	1·48	1·04	1·46	1·02	1·44
Xe	0·5	0·53	0·80	0·52	0·85	0·51	0·79
CCl_4	0·5	0·40	1·13	0·36	1·08	0·33	1·05
I_2	0·5	0·33	0·65	0·30	0·63	0·28	0·61
He	1·0	8·38	2·26	8·57	2·20	8·54	2·21
Air	1·0	—	1·49	—	1·46	—	1·43
Xe	1·0	0·49	0·77	0·46	0·74	0·44	0·72

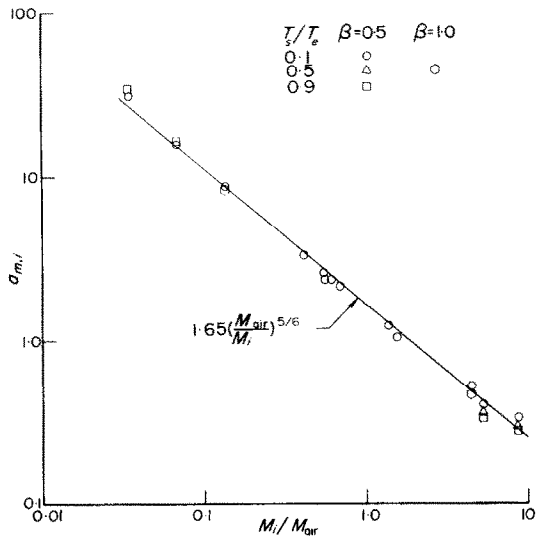

FIG. 10. Correlation of species weighting factors for mass transfer.

diatomic and polyatomic molecules, the ratio of C_{pi} to an equivalent monatomic value $\frac{5}{2}\mathscr{R}/M_i$ raised to a power suggests itself. A simple one-half power brings the air data into line, and as Fig. 11 shows, also works reasonably well for the other injectants. However it must be mentioned that the specific heat correction is best omitted for H_2O; this anomaly is due to the abnormal transport properties of the polar H_2O molecule. The final correlation recommended is then

$$a_{h,i} = 1{\cdot}3\left(\frac{M_{air}}{M_i}\right)^{\frac{1}{3}}\left(\frac{C_{pi}}{\frac{5}{2}\mathscr{R}/M_i}\right)^{\frac{1}{2}}. \qquad (27)$$

Some comments on the use of the correlation formulae, equations (20) and (21) are appropriate. Mass transfer data are most useful in mass transfer coefficient form, i.e. as a mass transfer conductance $g_{m,i} \equiv j_{1,s}/(m_{i,s} - m_{i,e})$. In analytical studies, such as the present one, it is convenient to specify the rate of injection of the foreign species; then in solving the species equation the resulting surface concentration $m_{1,s}$ is obtained. Previous studies, e.g. [1, 2], have presented data for $m_{1,s}$. But the most common technical problems are, for example, (i) determination of the mass loss from a vaporizing surface; here $m_{1,s}$ is the equilibrium concentration corresponding to the surface temperature, and (ii) determination of the reaction rate of a heterogeneous reaction; here $m_{1,s}$ may be zero (diffusion controlled limit), or may be implicitly determined by the kinetics of the chemical reaction. In both cases the relation between diffusive flux $j_{1,s}$ and concentration

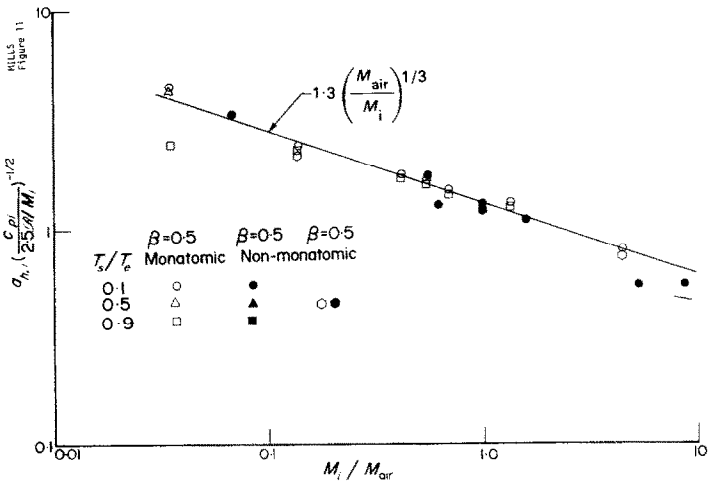

FIG. 11. Correlation of species weighting factors for heat transfer.

difference $(m_{1,s} - m_{1,e})$ is required, i.e. the mass transfer conductance. The effect of injection rate $\dot{m}$ is then conveniently exhibited by the ratio $g_{m,i}/g^*_{m,i}$.

The heat transfer to a surface through which mass transfer is taking place, is simply the conduction component of the surface energy flux, $q_s \equiv -k\,\partial T/\partial y|_s$, as can be most easily seen if we consider transpiration cooling from a reservoir of enthalpy $h_{1,0}$; an energy balance yields

$$q_s = -k\frac{\partial T}{\partial y}\bigg|_s = \dot{m}(h_{1,s} - h_{1,0}), \qquad (28)$$

i.e. the enthalpy rise of the coolant is equal to the conductive heat flux. If the thermal diffusion factor α_T is not assumed zero, then the diffusional conduction $j_1\alpha_T(M/M_1M_2)\,T|_s$ must be added to $-k\,\partial T/\partial y|_s$ in equation (28). Heat transfer data are then conveniently presented in the form of a heat transfer conductance $g_h \equiv -k\,\partial T/\partial y|_s/(H_e - h_{es})$, or Stanton number $St_h = g_h/\rho_e u_e$. Use of the enthalpy h_{es} ensures that the ratios g_h/g^*_h and St_h/St^*_h are identical to q_s/q^*_s, and yield the appropriate driving potential in the unity Lewis number limit.

ON THE USE OF MASS TRANSFER RESULTS FOR THE PREDICTION OF HEAT TRANSFER

In Appendix C of their review paper on laminar binary boundary layer characteristics, Gross *et al.* [18] evaluate the practice of equating a value of St^*_m experimentally determined using materials which sublime or evaporate such as naphthalene or water, to St^*_h (with or without a Lewis number correction). In their Fig. 37 appear curves of St_m/St^*_m which are quite different in character to those in Fig. 1b of the present paper; the source of the discrepancy is their incorrect definition of the mass transfer Stanton number as $\dot{m}/\rho_e u_e(m_{1,s} - m_{1,e})$, rather than $j_{1,s}/\rho_e u_e(m_{1,s} - m_{1,e})$. With this definition the ratio St_m/St^*_m for H_2O and CO_2 remains fortuitously close to unity, and for heavy injectants attains values much in excess of unity. The authors conclude that, whereas for H_2O and CO_2 St_m could well be interpreted as the solid wall St^*_h, for other gas mixtures considerable error would arise in the use of such a procedure.

Comparison of Figs. 2 and 3 of the present paper shows that, if the mass transfer Stanton number is correctly defined, the essential analogy between mass and heat transfer is preserved, i.e. St_m will equal St_h in the constant property and unity Lewis number limit. Thus we suggest that our correlations can be used to predict heat transfer from experimental mass transfer data; in so doing both the effects of injection ($St \neq St^*$) and variable properties will be accounted for in a rational manner.

CONCLUDING REMARKS

We have obtained comprehensive numerical solutions for axisymmetric and planar stagnation point flows of air with foreign gas injection. By considering a wide variety of injectants, including monatomic and non-monatomic molecules, as well as synthetic models, we have been able to explain the effect of injectant thermodynamic and transport properties on the reduction, due to mass transfer, of wall shear stress, mass transfer conductance and heat transfer rate. The increased pressure gradient at planar stagnation points is found to yield mass and heat transfer data which are little different to those for the axisymmetric situation. Engineering correlations for mass and heat transfer have been developed; these are of the exponential form suggested by a Couette flow model, with suitable weighting of the blowing parameter. The correlations apply to monatomic, diatomic and polyatomic molecules, for a large range of wall cooling, and both axisymmetric and planar stagnation points.

REFERENCES

1. J. R. Baron, Thermal diffusion effects in mass transfer, *Int. J. Heat Mass Transfer* **6**, 1025–1033 (1963)
2. E. M. Sparrow, W. J. Minkowycz and E. R. G. Eckert, Diffusion-thermo effects in stagnation-point flow of air with injection of gases of various molecular

weights into the boundary layer, *AIAA Jl* **2**, 652–659 (1964).
3. P. A. LIBBY and P. SEPRI, Stagnation point flow with complex composition, *Physics Fluids* **11**, 1621–1627 (1968).
4. N. A. ANFIMOV, Heat and mass transfer near the stagnation point with the injection and suction of various gases through the body surface, *Mekh. Zhid. Gaza* **1**, 22–31 (1966).
5. A. V. GOMEZ, A. F. MILLS and D. M. CURRY, Correlations of heat and mass transfer for the stagnation region of a re-entry vehicle with multicomponent mass addition, *Space Systems and Thermal Technology for the 70's*, Part II, ASME (June 1970).
6. A. F. GOLLNICK, JR., An experimental study of thermal diffusion effects on a partially porous mass transfer-cooled hemisphere, *Int. J. Heat Mass Transfer* **7**, 699–708 (1964).
7. M. W. RUBESIN and C. C. PAPPAS, An analysis of the turbulent boundary-layer characteristics on a flat plate with distributed light gas injection, NACA TN 4149 (1958).
8. J. O. HIRSCHFELDER, C. F. CURTISS and R. B. BIRD, *Molecular Theory of Gases and Liquids*, 2nd ed. Wiley, New York (1964).
9. L. LEES, Laminar heat transfer over blunt-nosed bodies at hypersonic flight speeds, *Jet Propulsion* **26**, 259–269 (1956).
10. R. A. SVEHLA, Estimated viscosities and thermal conductivities of gases at high temperatures, NASA TR R132 (1962).
11. P. A. LIBBY and P. SEPRI, Laminar boundary layer with complex composition, *Physics Fluids* **10**, 2138–2146 (1967).
12. E. T. DERGAZARIAN *et al.*, *JANAF Thermochemical Tables*. The Dow Chemical Co., Midland, Mich. (1960 and supplements to date).
13. A. WORTMAN, Mass transfer in self-similar laminar boundary layer flows, Ph.D. Dissertation, School of Engineering and Applied Science, University of California, Los Angeles (1969).
14. A. WORTMAN and A. F. MILLS, Highly accelerated compressible laminar boundary-layer flows with mass transfer, *J. Heat Transfer* **93**, 281–289 (1971).
15. H. HOSHIZAKI and H. J. SMITH, Axisymmetric stagnation point mass-transfer cooling, Lockheed Missiles and Space Division, TR LMSD-48379 (December 1958).
16. D. B. SPALDING, *Convective Mass Transfer*. Edward Arnold, London (1963).
17. W. M. KAYS, *Convective Heat and Mass Transfer*. McGraw-Hill, New York (1966).
18. J. F. GROSS, J. P. HARTNETT, D. J. MASSON and C. GAZLEY JR., A review of binary laminar boundary layer characteristics, *Int. J. Heat Mass Transfer* **3**, 198–221 (1961).

ECOULEMENTS BIDIMENSIONNELS D'UN MÉLANGE BINAIRE AUTOUR D'UN POINT D'ARRÊT

Résumé—Des solutions numériques générales ont été obtenues pour des écoulements d'air axisymétriques et plans autour d'un point d'arrêt avec injection d'un gaz différent. Les espèces injectées sont H, H_2, He, C, CH_4, O, H_2O, Ne, Air, Ar, CO_2, Xe, CCl_4 et I_2 pour des rapports de refroidissement pariétal T_s/T_e = 0,1 ; 0,5 et 0,9. On a calculé les propriétés thermodynamiques en supposant un mélange de gaz inerte idéal et des chaleurs spécifiques constantes ; pour les propriétés de transport, on utilise un modèle de sphère rigide afin d'éliminer le niveau de température comme paramètre du problème. Les effets sur la réduction, due au transfert massique, des propriétés thermodynamiques et de transport de la contrainte tangentielle, de la conductance du transfert massique et du flux thermique sont expliqués à l'aide de résultats calculés pour des gaz injectés théoriques ayant des chaleurs spécifiques et des sections efficaces ajustées. On trouve que l'accroissement du gradient de pression à des zones d'arret planes ($\beta = 1$) donne des résultats peu différents de ceux relatifs à la situation axisymétrique ($\beta = 0{,}5$) excepté en ce qui concerne la réduction de contrainte tangentielle pour des gaz injectés légers à des températures pariétales élevées. On trouve intéressant les effets de diffusion thermique avec un refroidissement à la paroi modéré ou sévère, mais de peu d'importance pratique. On présente des relations utilisables pour le transport massique et thermique. Elles sont de forme exponentielle suggérée par un modèle d'écoulement de Couette avec le paramètre de soufflage B adapté par des facteurs :

$$a_{m,i} = 1{\cdot}65 \left(\frac{M_{air}}{M_i}\right)^{\frac{1}{3}}; \qquad a_{h,i} = 1{\cdot}3 \left(\frac{M_{air}}{M_i}\right)^{\frac{1}{3}} \left(\frac{C_{pi}}{\frac{5}{2}\mathscr{R}/M_i}\right)^{\frac{1}{3}}$$

respectivement pour les transferts massique et thermique.

ZWEIDIMENSIONALE STAUPUNKTSTRÖMUNG VON ZWEISTOFFGEMISCHEN

Zusammenfassung—Es ergaben sich umfassende numerische Lösungen für achssymmetrische und ebene Staupunktströmung von Luft mit Fremdgasinjektion. Die injezierten Gase sind H, H_2, He, C, CH_4, O, H_2O. Ne, Luft, Ar, CO_2, Xe, CCl_4 und I_2, bei Wandkühlungsraten von T_s/T_e = 0,1, 0,5 und 0,9. Die thermodynamischen Eigenschaften wurden unter der Annahme einer idealen Inert-Gasmischung und

konstanter spezifischer Wärmer berechnet; für die Transportgrössen wurde das starre Kugel-Modell angewendet, um das Temperaturniveau als Parameter zu eliminieren. Der Einfluss der thermodynamischen und der Transporteigenschaften des eingespritzten Anteils auf die Verminderung der Wandschubspannung, gemäss dem Massentransport, auf die Verminderung der Massentransportgrösse und der Wärmeübergangsrate, wird erklärt mit Hilfe von Ergebnissen, die für synthetische Einspritzmedien mit angepasster Wärmeleitfähigkeit und angepassten Stoss-Querschnitten berechnet sind. Es zeigte sich, dass der höhere Druckgradient an ebenen Staupunkten ($\beta = 1{,}0$) eine leichte Abweichung der Ergebnisse bewirkt, gegenüber denen der achssymmetrischen Anordnung ($\beta = 0.5$) ausser bei Schubspannungsverminderung mit leichten Injektionsmitteln bei hohen Wandtemperaturen. Einflüsse thermischer Diffusion bei mässiger bis starker Wandkühlung erwiesen sich als interessant, doch von geringer praktischer Bedeutung. Ingenieurmässige Beziehungen für Massen- und Wärmetransport werden angegeben. Sie haben exponentielle Form, nach einem Couette-Strömungsmodell; mit dem Anblasparameter B, der von den Faktoren

$$a_{m,i} = 1{,}65\left(\frac{M_{i_w f i}}{M_i}\right)^{\frac{1}{3}};\ a_{h,i} = 1{,}3\left(\frac{M_{i_w f i}}{M_i}\right)^{\frac{1}{3}}\left(\frac{C_{pi}}{\frac{5}{2}\mathscr{R}/M_i}\right)^{\frac{1}{3}}$$

für Massen- und Wärmetransport bestimmt wird.

ДВУМЕРНЫЕ ПОТОКИ БИНАРНЫХ СМЕСЕЙ В КРИТИЧЕСКОЙ ТОЧКЕ

Аннотация—Получены численные решения для осесимметричных и плоских потоков воздуха в критической точке при вдуве инородного газа. Вдувались следующие вещества: H_2, He, C, CH_4, O, H_2O, Ne, воздух, Ar, CO_2, Xe, CCl_4 и I_2 при коэффициенте охлаждения равном $T_s/T_e = 0{,}1$; 0,5. Рассчитаны термодинамические свойства при допущении инертной идеальной газовой смеси и постоянной удельной теплоемкости образца; для исключения температурного уровня из параметров задачи используется модель жесткой сферы. Влияние термодинамнческих свойств вдуваемых веществ на уменьшение напряжения трения на стенке за счет массообмена, массопроводность и интенсивность теплообмена объясняются с помощью численно полученных результатов для синтетических вдуваемых веществ при соответствующих значениях удельной теплоемкости и сечениях соударений. Найдено, что повышенный градиент давления в критических точках для плоских течений ($\beta = 1{,}0$) приводит к результатам, которые незначительно отличаются от результатов для осесимметричного случая ($\beta = 0{,}5$) за исключением уменьшения напряжения сдивига при вдуве лёгких веществ при больших температурах на стенке. Оказывается, что эффект термодиффузии при степенях охлаждения стенки от умеренных до предельных представляют интерес, хотя и имеют незначительное практическое значение. Представлены инженерные формулы связи процесса тепло- и массопереноса. Эти формулы имеют экспоненциальный вид для модели куэттовского течения при параметре вдува B, отнесенным к коэффициентам тепло- и массообмена

$$a_{m,i} = 1{,}65\left(\frac{M_{\text{air}}}{M_i}\right)^{\frac{1}{3}}\ ;\ a_{h,i} = 1{,}3\left(\frac{M_{\text{air}}}{M_i}\right)^{\frac{1}{3}}\left(\frac{C_{pi}}{\frac{5}{2}\mathscr{R}/M_i}\right)^{\frac{1}{3}}$$